RSC Advances

ROYAL SOCIETY OF CHEMISTRY

www.rsc.org/advances

Coal fly ash industrial waste recycling for fabrication of mullite-whisker-structured porous ceramic membrane support

Li Zhu[a, b], Yingchao Dong[a, b] *, Lingling Li[a,b,c], Jing Liu[a,b,c], Sheng-Jie You[d]

With recyclable industrial waste coal fly ash and bauxite as starting materials, porous mullite-whisker-structured ceramic membrane supports were fabricated at sintering temperatures ranging from 1100 to 1400 °C with addition of AlF_3 and MoO_3 as mineralizer and crystallization catalyst, respectively. Dynamic sintering of mullite membrane supports was first studied. Then the characterizations were focused on open porosity, pore size distribution, gas flux and mechanical properties, microstructure and phase evolution. It shows that introduction of MoO_3 effectively promoted the growth of elongated mullite crystal in membrane support by reducing the high temperature viscosity of the liquid melt. Addition of 5 wt. % MoO_3 lowered secondary mullitization temperature, resulting in more mullite formation at temperature as low as 1200 °C, while porosity of 45.4±0.9% was obtained. After sintering at 1200 °C, open porosity was 47.3±0.6% for the sample containing 4 wt. % AlF_3. The co-introduction of MoO_3 and AlF_3 promoted formation of a whisker-interlocked porous structure, which effectively improved open porosity and permeation flux without significant mechanical strength degradation.

1. Introduction

Million of tonnes of industrial solid state waste coal fly ash are generated worldwide as it is a by-product of coal combustion in power plants. It is estimated that more than 750 million tonnes is produced per annum, but only less than 50% of global flyash production is utilized [1]. In China, the yield of fly ash as the solid state waste by-product of power generation exceeds 200 million tonnes in 2009 [2]. Currently, fly ash produced in China has mainly been used in some applications with low economic benefits, e.g. in brick manufacturing and road or dam construction. Nevertheless, large amounts of fly ash are still dumped into ponds or piled on land [3] which can be regarded as unsightly, environmentally undesirable [4] or a non-productive use of land resources, as well as posing an on-going financial burden through their long-term maintenance. It is now widely realized that fly ash should be considered as a useful and potential mineral resource and therefore the development of high value-added utilization technologies of fly ash is quite important. Environment-friendly utilization of coal fly ash is an important subject because of the measures needed for the prevention of environmental pollution. During the last decade, some researchers have tried to recycle coal fly ash for preparation of ceramic membranes and function materials, such as microfiltration membranes [5-7], zeolites [8], and sorbents [9].

Porous ceramic membranes are used in many industrial fields due to their unique advantages, such as excellent thermal stability, good pressure resistance and good antifouling properties [10]. However, high cost commercial porous ceramic membranes (such as Al_2O_3, ZrO_2, SiO_2, TiO_2) [11] cannot fulfill environmental requirements such as separation in strong alkaline media and massive liquid waste treatment. Porous mullite is a potential candidate as support for ceramic membrane because it has a high melting point (1830 °C), good chemical durability and sufficient mechanical strength [12].

The fly ash with main compositions Al_2O_3 and SiO_2 is especially suitable for the fabrication of mullite-based ($3Al_2O_3{\cdot}2SiO_2$) ceramics. Synthesized mullite can have any composition between x= 0 (sillimanite) and x=1 (alumina) in a general formula $Al_{4+2x}Si_{2-2x}O_{10-x}$, dependant on starting material and processing route [13, 14]. There are some renewed interests in the conversion of coal fly ash to dense mullite and porous mullite. Guo et al. [15] focused on preparation of mullite from desilication-flyash, and described the inner structure of flyash and the growth of mullite crystal. Jung et al. [16] successfully synthesized 3YSZ-doped mullite ceramics from waste fly ash and submicron sized Al_2O_3 powders with the addition of 3YSZ. Li et al. [17] synthesized V_2O_5-doped mullite from coal fly ash. Li et al. [18] fabricated porous mullite ceramics from flyash, investigating the mechanical strength with different aluminium sources. Huang et al. [19] reported the preparation of mullite using a mixture of fly ash and alumina. The high performance mullite whiskers can be synthesized from the coal fly ash and this is of commercial interests and environmental implications [20]. Generally, mullite formation by conventional methods such as simple sintering of alumina and silica powders requires a full crystallization temperature as high as ~ 1500-1600 °C. As a result, extensive efforts are made to achieve lower mullitization temperature and to enhance mullite phase content in the matrix. Additives like V_2O_5 [17], and MgO [21] are used as mineralizers to reduce the sintering temperature. In the present work, a new processing route is applied to directly make porous mullite support for ceramic membrane using coal fly ash and bauxite with the addition of AlF_3 and MoO_3 to reduce sintering temperature, as well as to change pore-structure.

Normally, an improvement in open porosity, which is required to endow a low fluid resistance, is achieved with addition of pore-forming agents such as graphite powder or some organic compounds [22, 23], which are burned-out or decompose completely during heating. However, the pores produced in this way are usually believed to deteriorate the mechanical reliability [24]. In order to improve mechanical property, many efforts have accordingly been made to toughen porous mullite ceramics with different methods, such as particle dispersion reinforcement [25] and whisker or fiber toughening [26, 27]. Among these methods, whisker toughening is an effective approach to strengthen the material. Therefore, in this work, an *in situ* synthesis method has been adopted to fabricate porous ceramic membrane support entirely composed of interlocked whiskers during the sintering process.

In this work, with industrial waste coal fly ash and bauxite as starting materials, a highly porous structure composed of interlocked *in situ* synthesized mullite whiskers is created in a mullite membrane support using AlF_3 and MoO_3 as additives. The effects of additives and sintering parameters on the main properties of as-prepared porous mullite membrane supports were studied in detail, mainly including thermal analysis, porosity, pore size and gas flux, mechanical properties, micro-structure (SEM-EDS, TEM-SAED), and phase compositions (XRD). The present study aims at recycling of industrial waste fly ash for fabrication of a whisker-structured porous ceramic membrane support with increased porosity and flux, but without significant degradation of mechanical property.

2. Experimental

2.1. Starting materials for membrane support

The coal fly ash and bauxite were obtained from Beilun thermal power plant (Ningbo, Zhejiang Province,

China) and Yangquan (Yangchuan, Shanxi Province, China), respectively. AlF_3 (98%-102%, Guangfu Fine Chemical Reagent Ltd., Tianjin, China) and MoO_3 (Sinopharm Chemical Reagent Co., Ltd) were used as crystallization catalyst and mineralizer, respectively. The chemical compositions of the coal fly ash and bauxite were analyzed by an X-ray fluorescence spectrometer (WDXRF, PANalytical Corporation, Netherlands) and date are summarized in Table 1. The coal fly ash contains 44.76 wt. % Al_2O_3 and 44.17 wt. % SiO_2.

Table 1 Main chemical composition (wt. %) of fly ash and bauxite measured by semi-quantitative XRF.

Materials	Chemical composition (%)								
	Al_2O_3	SiO_2	CaO	Fe_2O_3	TiO_2	SO_3	K_2O	Na_2O	Others
fly ash	44.76	44.17	4.57	3.02	1.92	0.44	0.4	0.22	0.49
bauxite	63.53	10.41	0.47	7.08	2.98	0.18	0.28	0.15	0.52

The loss on ignition of fly ash and bauxite is 1.01 and 14.40 wt. %, respectively

Based on the results of the XRF analysis, bauxite (63.53 wt. % Al_2O_3 and 10.41 wt. % SiO_2) was added to the coal fly ash in order to compensate for a deficient alumina composition as compared to stoichiometric mullite ($3Al_2O_3 \cdot 2SiO_2$). In addition, AlF_3 and MoO_3 were added to the mixture of coal fly ash and bauxite. Here, AlF_3 was also consumed as partial aluminum source to form stoichiometric 3:2 mullite via its transformation to Al_2O_3, followed by reaction with SiO_2. All the samples were labeled as AxMy hereafter in this paper. A stands for AlF_3, M for MoO_3, and the numbers following them represent their mass percents in the samples (e.g. A0M0 for the sample without addition of AlF_3 and MoO_3, A4M5 for the sample with addition of 4 wt. % AlF_3 and 5 wt. % MoO_3).

2.2. Fabrication of membrane support

The raw materials were wet-ball-milled and dried at 100 °C for 12 h, After complete drying, the milled powders were uniformly mixed with organic binder PVA-1750 (5.0 wt. % solution) and then uniaxially pressed into cylindrical pellets (20mm in diameter and 1~2 mm in thickness) and rectangular bars (40mm× 7mm × 3~4 mm) at a pressure of 190 MPa. Then the green samples were respectively placed in a closed alumina crucible and sintered in a muffle furnace in air (at 1100-1400 °C).

2.3. Preparation and separation of oil-in-water emulsions

The surfactant-stabilized oil-in-water emulsions were prepared by mixing soybean oil with water in a volume ratio of 1:99. Sodium dodecyl sulfonate with a concentration of 0.05 mg/mL was added into the mixture as an emulsifier. Then ultrasonication of the mixtures for 1 h produced a white and milky solution.

2.4. Characterization and test

The particle size distribution of fly ash and bauxite was determined by a laser particle size analyzer (Mastersizer 2000, Malvern Instruments Ltd., UK). The dynamic sintering behaviors of the green rectangular bars (A0M0, A4M0, A0M5 and A4M5) were studied in a horizontal dilatometer (DIL 402C, Netzsch, Germany) with an operating temperature of room temperature (25 °C) to 1500 °C and a constant heating rate of 10 °C•min^{-1}. Micro-region compositional analysis was performed using an energy dispersive spectrometer (EDS, Genesis XM2, EDAX, LTD., America) combined with SEM (SEM, S-4800, Hitachi Ltd., Japan). Phase analysis was identified by X-ray diffraction (XRD, D8 advance, Bruker Corporation, Germany). Here, XRD semi-quantitative analysis based on the normalized reference intensity ratio (RIR) method was adopted to calculate the mullite content in the sintered samples [28]. The mullite crystal structure was investigated by SAED (selected-area electron diffraction) based on TEM (JEM-2010; JEOL, Tokyo, Japan).

Open porosity was determined by the Archimedes method with water as the liquid medium. Pore size distribution of the mullite membrane supports was measured by a pore size distribution analyzer (PSDA-20, Nanjing Gaoqian function materials Co. Ltd., China) based on a gas-liquid displacement method [29]. A home-made flow setup was used for N_2 flux study and oil-in-water emulsion separation. The samples were clamped in a brass fixture, the inlet side of the test fixture was operated in a dead-end mode with the inlet pressure controlled by means of a pressure regulator and a digital pressure gauge. The feed and permeation samples were analyzed by the total organic carbon meter (TOC-Vcph).

Biaxial flexural strength (BFS) and three point bending strength σ were measured by a universal testing machine (AGS-X, Shimadzu Ltd., Japan). BFS was calculated using the following formula for maximum tensile stress given by Timoshenko et al. [30].

$$BFS(MPa)= N/ t^2 \{(1+v)[(0.485\ln(a /t)+ 0.52]+ 0.48\} \quad (1)$$

Where N is the load (N), ν is Poisson's ratio (ν=0.26 in this study), a is the radius of the support (m) and t is the thickness of the specimen (m).

The mechanical reliability was tested by applying the well known Weibull statistics to the experimental data [31].

According to Weibull statistics, the increasing probability of failure (P_f) for a brittle material can be expressed by

$$P_f = 1 - \exp\left(-(\sigma/\sigma_0)^m\right) \quad (2)$$

Where P_f is the failure probability for an applied stress (σ) as mentioned above, σ_0 is a normalized parameter known as Weibull characteristic strength, and m is the Weibull modulus. Here, the Weibull modulus is a measure of the degree of strength data dispersion. Three point bending strength (σ) was calculated according to the following expression (ISO9693 1999).

$$\sigma = \frac{3P \times l}{2b \times h^2} \quad (3)$$

where (σ) is fracture strength (Pa), P is fracture load (N), l is span length (m, l= 30 mm in this study), b is width of sample (m), h is height of sample (m).

3. Results and discussion

3.1. Characterization of starting materials

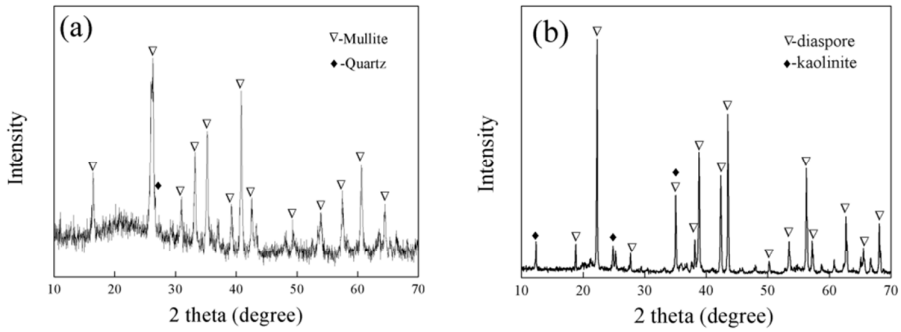

Fig. 1 XRD patterns of two starting materials: (a) coal fly ash, (b) bauxite.

Fig.1 displays the XRD patterns of fly ash and nature bauxite. As shown in Fig. 1a, coal fly ash mainly consists of mullite ($3Al_2O_3 \cdot 2SiO_2$, PDF#15-0776) and quartz (SiO_2, PDF#99-0088). The mullite existing in the fly ash belongs to primary mullite, which is formed from aluminosilicate clay minerals during the combustion process of raw coal, the percentages of mullite and quartz are 49% and 51% respectively based on RIR analysis. Fig. 1b presents the XRD pattern of bauxite. The major crystalline phases detected are diaspore (AlO(OH), PDF#99-0044) and kaolinite ($Al_2O_3 \cdot 2SiO_2 \cdot 2H_2O$, PDF#99-0067). The content of mullite in the precursor mixture of coal fly ash and bauxite is 18% based on RIR method.

The mean particle diameters of coal fly ash and bauxite powders (Fig. 2a) are 2.12 μm and 1.22 μm after ball-milling for 12 h, respectively. The fly ash powder consists mainly of silicate minerals, a mixture of flake-like and nearly spherical-shaped particles (Fig. 2b). While bauxite powder has an irregular shape with the presence of some fine particles (Fig. 2c).

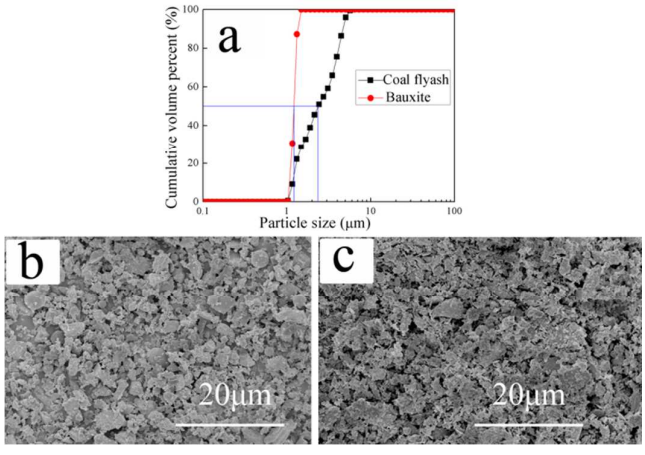

Fig. 2 Particle size distributions (a), SEM images of coal fly ash (b) and bauxite (c) after ball-milling

3.2 Sintering and pore structure

3.2.1 Dilatometric measurement

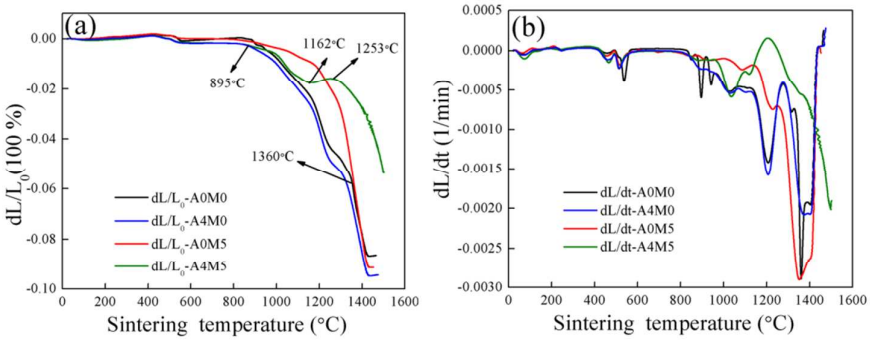

Fig. 3 Linear shrinkage percent dL/dL_0 (a) and sintering shrinkage rate dL/dt (b) of the membrane supports: A0M0, A4M0, A0M5 and A4M5.

Fig. 3 illustrates the dynamic sintering curves, based on a dilatometric test, of the green membrane supports. At first stage (420-580 °C) the dehydroxylation of kaolinite and diaspore take place successively for all the samples. The second stage of densification starts at a low rate over 895-1100 °C for the sample without addition (A0M0). The sintering of some high-activity fine fly ash and bauxite particles causes this slight shrinkage. The sample with AlF_3 (4 wt. %) addition (A4M0) exhibits similar sintering shrinkage behaviors with that without addition (A0M0). By contrast, the sample (A0M5) with MoO_3 (5 wt. %) addition and the sample containing both AlF_3 and MoO_3 (A4M5) exhibits different sintering shrinkage behaviors from these without MoO_3 (A0M0, A4M0). The A0M5 sample exhibits obvious lower shringkage compared with A0M0 and A4M0. Unlike A0M0 and A4M0, the initial shrinkage is delayed to higher temperature for all the samples with MoO_3 addition. The initial shrinkage temperature is about 1200 °C for the A0M5 membrane supports which is much lower than these of A0M0 and A4M0. It is concluded that with addition of MoO_3, the mullitization-crystal-growth process is obviously improved (will be verified by the following XRD results, Fig.11) at temperature below 1200 °C, which inhibits the shrinkage of the sample at low temperatures.

For A4M5, the first stage, with only a very slight densification, occurs over a lower temperature range of 895-1162 °C, and then a unique significant sintering self-expansion stage is observed from 1162 to 1253 °C. At this stage, the secondary mullitization reaction is caused by the dissolution of corundum into transient glassy liquid phase, followed by the precipitation of mullite crystals [32]. It suggests that this mullitization-crystal-growth process is induced at much lower temperature than these without additives, and significantly accelerated as a result of the addition of AlF_3 and MoO_3. The volume expansion caused by this mullitization-crystal-growth process was also mentioned in fly ash-bauxite in our previous study, where the self-expansion stage was from 1326 °C to 1477 °C [33].

3.2.2 Open porosity

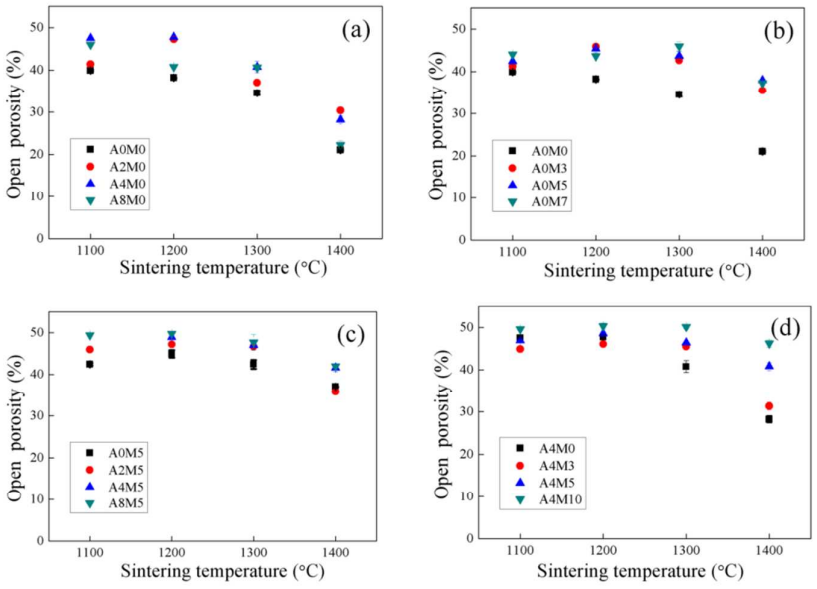

Fig. 4 Open porosity of the membrane supports with various contents of AlF_3 and MoO_3 as a function of sintering temperature.

Fig. 4 shows the open porosity of the membrane supports with various contents of AlF_3 and MoO_3 as a function of sintering temperature. The presence of AlF_3 and MoO_3 causes different changes in open porosity. The porosity increases with AlF_3 content (Fig. 4a) when sintering at the same temperature between 1100-1400 °C. The samples sintered at 1200 °C exhibit the highest open porosities with 4.0 wt. % AlF_3. The open porosities are respectively 38.2±0.1%, 47.3±0.6%, 47.8±0.4% and 40.8±0.4% for the samples containing 0 wt. %, 2 wt. %, 4 wt. % and 8 wt. % AlF_3. It shows that addition of 4 wt. % AlF_3 is the optimum at 1200 °C. At all the investigated sintering temperatures (1100-1400 °C), the porosity increases with increasing MoO_3 content (Fig. 4b) (0 wt. %, 3 wt. % and 5 wt. %), the open porosity is 45.4±0.9% for the samples containing 5 wt. % MoO_3 sintered at 1200 °C.

The combined effects of the AlF_3 and MoO_3 content and the sintering temperatures on the porosity are illustrated in Figs. 4c and 4d. It can be found that the open porosity decreases with increasing temperature because of the gradual densification induced by sintering, except for 1200 °C due to a mullitization-crystal-growth induced volume expansion, which is consistent with the above-mentioned dynamic sintering result of A4M5 (see Fig. 3).

In all cases, open porosity does not change much as the AlF_3 content in samples increases from 0 to 8 wt. % when the MoO_3 content keeps constant. But open porosity increases with increasing MoO_3 content with addition of the same content of AlF_3 (4 wt. %), indicating that addition of MoO_3 is more effective in enhancing open porosity of mullite membrane supports than addition of AlF_3. It suggests that MoO_3 effectively promotes the mullitization-crystal-growth process, which is further supported by SEM result (see Fig. 8).

3.2.3 Pore size distribution

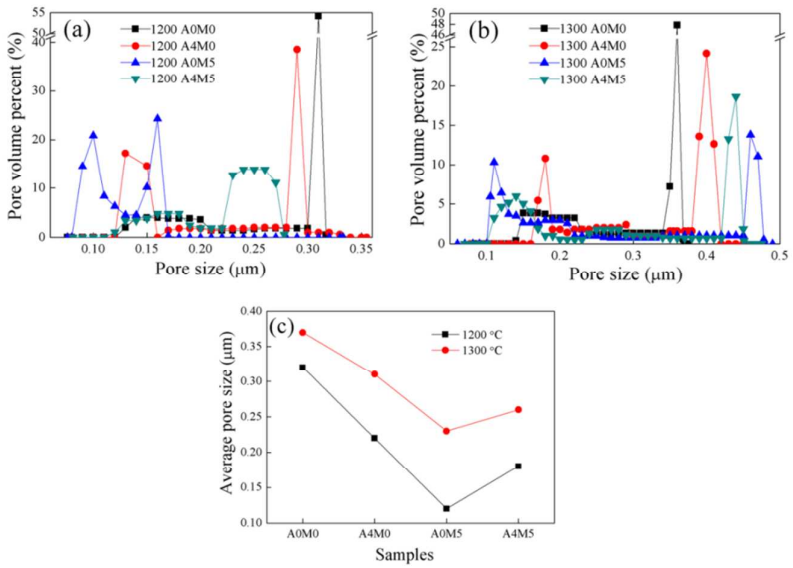

Fig. 5 Pore size distributions (a, b) and average pore size (c) of the A0M0, A4M0, A0M5 and A4M5 membrane supports sintered at 1200 °C and 1300 °C.

Fig. 5 presents the pore size distributions and average pore size of the A0M0, A4M0, A0M5 and A4M5 membrane supports sintered at 1200 °C and 1300 °C. The pore size distribution curve shifts to large pore size for all the membrane supports (Fig. 5a and Fig. 5b) and an increase in average pore size is observed (Fig. 5c) from 1200 °C to 1300 °C. The A0M0 membrane supports show a unimodel distribution of pore size, the average pore sizes of A0M0 (Fig. 5c) are found to be 0.32 and 0.37 μm after sintering at 1200 °C and 1300 °C, due to the sintering-induced growth of mixture particles leading to the formation of large pores and elimination of small pores at high temperature. These trends are similar with the mullite membrane supports prepared in our previous work [33].

Compared with A0M0, with addition of AlF_3 and MoO_3, the mean pore sizes of A4M0, A0M5 and A4M5 become smaller. These membranes supports exhibit bimodal distributions of pore size, which are probably due to the formation and growth of stiff skeleton needle-like mullite crystals (i.e. mullite whiskers), resulting in formation of some much finer pores among them [34].

3.2.4 Nitrogen gas flux across membrane supports

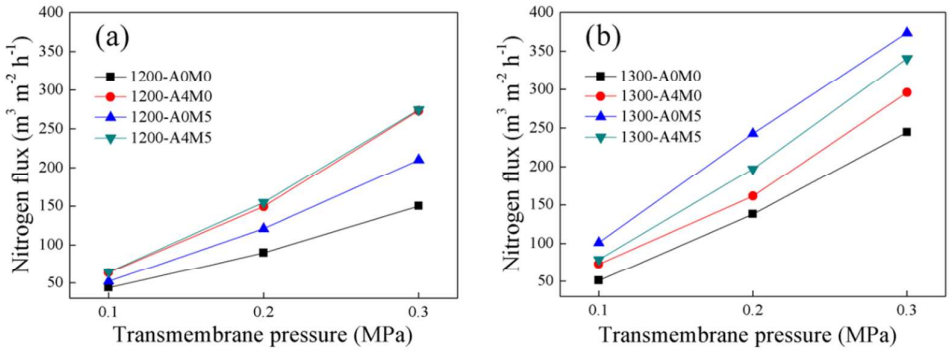

Fig. 6 Nitrogen gas flux of A0M0, A4M0, A0M5 and A4M5 membrane supports sintered at 1200 °C and 1300 °C (measured at room temperature: 25 °C).

Fig. 6 shows nitrogen gas flux of ceramic membrane supports sintered at 1200 °C and 1300 °C. For all the samples, the nitrogen gas flux (Fig. 6) increases from 1200 to 1300 °C, the higher flux of samples at 1300 °C may be correlated to a "pore growth" phenomenon. When a gas flows across porous membranes dominated by the viscous flow mechanism, gas flux is proportional to open porosity and the square of pore size according to the Hagen-Poiseuille equation [35].

$$J_V = \frac{\varepsilon r^2}{8\eta\tau}\frac{\Delta P}{\Delta x} \quad (4)$$

Where J_V stands for the membrane volume flux, ε for the open porosity, r for the pore size, η for the viscosity, τ for the tortuosity factor, $\Delta P/\Delta x$ for the pressure gradient. Therefore, an increase in pore size is more beneficial to increase gas flux across a porous membrane than open porosity. This is verified by the observation that the gas flux is higher for the samples sintered at 1300 °C, which have a larger pore size.

With addition of AlF_3 and MoO_3, A4M0, A0M5 and A4M5 membrane supports always exhibit higher nitrogen gas flux than A0M0 at the same temperatures despite their smaller mean pore size (see Fig. 5). This improvement in gas flux may be ascribed to a microstructural change of A4M0, A0M5 and A4M5 exhibiting a large number of open pores constructed by mullite whiskers, which are believed to be responsible for accelerating gas flow through the membrane supports.

3.3 Mechanical strength and microstructure analysis

3.3.1 Mechanical strength

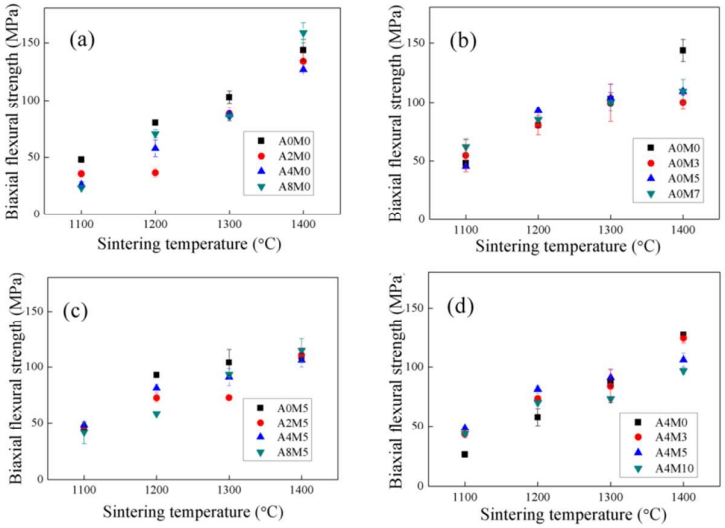

Fig. 7 Biaxial flexural strengths (BFS) of the membrane supports with various contents of AlF_3 and MoO_3 as a function of

sintering temperature

Fig. 7 shows the biaxial flexural strengths (BFS) of the membrane supports. As shown in Fig. 7, the strength gradually increases with increasing sintering temperature for all the samples. From 1100 to 1400 °C, the average biaxial flexural strength of all the AlF_3-doped (AxM0) (Fig. 7a) and MoO_3- doped (A0Mx) (Fig. 7b) samples increases from 26.2.±2.4 MPa to 158.7.±8.7 MPa and from 45.5±2.6 MPa to 109.4±10.0 MPa, when compared to A0M0 (from 48.1±2.5 MPa to 143.7±9.3MPa), suggesting that separate doping of AlF_3 and MoO_3 resulted in small difference in the strength of mullite membranes support. Although there is an increase in porosity with the combined addition of the AlF_3 and MoO_3, the samples show no degradation in mechanical strength at each temperature (Fig. 7c and Fig. 7d).

The co-introduction of AlF_3 and MoO_3 promoted formation of a novel porous whisker-interlocked structure (will be verified by the following SEM images), which effectively improves open porosity and gas flux without significant mechanical strength degradation.

To normalize the mechanical strength, whereby three point strength is also measured. A comparison between flexural strength values for the as-fabricated porous mullite membrane support in this work and these (carried out on silimar porous based ceramic) reported in the literatures [15, 17, 18, 33, 34] is shown in Table 2. This may lead to the following remarks: it has been found in the literature that flexural strength values were ranged between 36.05 MPa and 108 MPa when sintering at temperatures ranging between 1200 °C and 1550 °C. One can conclude that these reported values are in a good agreement with those found in this work. The flexural strength values in the present work are higher than these reported values after sintering at 1200 °C, and at a comparable level of these reported values after sintering above 1200 °C, it is important to note the mullite membrane supports in this work require lower temperature to obtain the same value of mechanical strength when compared to the literatures. Due to the addition of MoO_3 and AlF_3, there is a significant change in the microstructure of the fabricated mullite membrane support, which is entirely composed of interlocked mullite whiskers. The intergrown mullite whiskers could impart good mechanical strength and structure rigidity to the porous mullite support.

Table 2: Comparison between flexural strength values for the as-fabricated porous mullite membrane support in this work and these reported in the literature.

Material	Sintering temperature (°C)	Three point bending strength (MPa)	Phases	References
Fly ash+Bauxite	1450	36.05	Mullite+Corundum	33
Fly ash	1550	100	Mullite	18
Fly ash+Bauxite	1200	60.9±2.5	Mullite+Corundum	Present work
Fly ash+Bauxite	1300	68.3±5.7	Mullite+Corundum	Present work
Kaolin+Al_2O_3	1550	66.7	Mullite	34
Flyash	1400	<50	Mullite+Cristobalite	15
Fly ash+Bauxite	1500	108	Mullite	17
Fly ash+Bauxite	1200	<50	Mullite	17

3.3.2 Weibull analysis

Table 3 Weibull modulus (m) extracted from the flexural strength data for the samples sintered at 1200 and 1300°C.

Samples	1200-A0M0	1300-A0M0	1200-A4M5	1300-A4M5
Weibull modulus	38.5±3.9	17.68±1.2	22.1±3.6	38.9±3.0

Weibull statistics [36] is commonly used to describe the fracture behavior of brittle materials. Table 3 lists the Weibull modulus m for the A0M0 and A4M5 samples sintered at 1200-1300 °C. Weibull modulus, called the shape factor m, relates to the uniformity of the distribution of flaws in a brittle material: a high value of m (say, m>20) implies a highly uniform distribution of defect sizes and therefore a narrow range of fracture strengths. Conversely, a low value of m [37] (for example, m<2) implies highly variable flaws sizes and a large spread of measured strengths. The relatively high Weibull modulus in this work, m~17.6-38.9 (Table 3), means good mechanical reliability for the as-fabricated membrane samples.

3.3.3 SEM-EDS

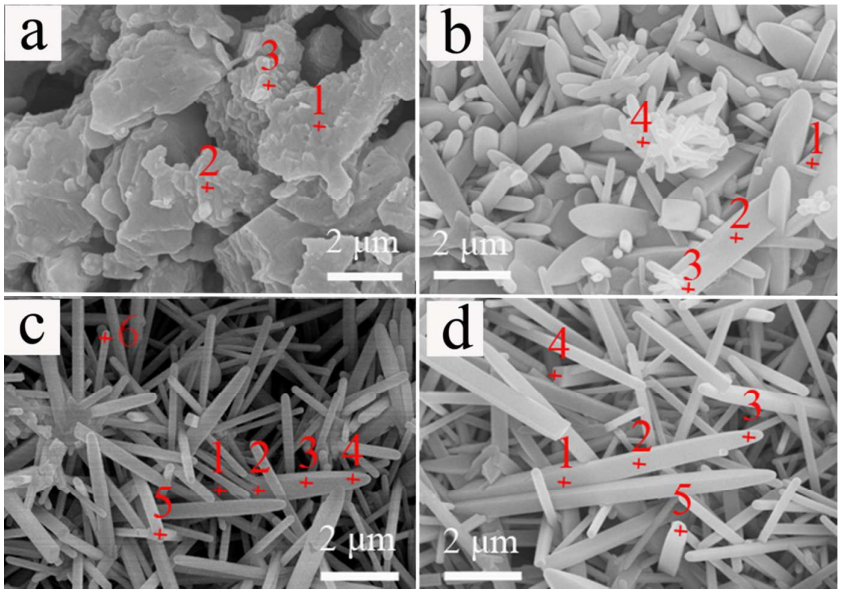

Fig. 8 SEM images of mullite membrane supports (a) A0M0-1200 °C, (b) A4M0-1200 °C, (c) A0M5-1200 °C and (d) A4M5-1200 °C

Table 4 EDS analysis of the A0M0, A4M0, A0M5 and A4M5 membrane supports sintered at 1200 °C (from Fig. 8).

Samples	Analysis area	at. % (average value)		Molar ratio Al/Si
		Al	Si	
A0M0	Spectra 1- 3	40.3±3.6	16.4±3.8	2.5
A4M0	Spectra 1- 4	43.2±4.6	11.4±0.5	3.8
A0M5	Spectra 1- 3	41.4±5.1	13.2±2.4	3.1
A4M5	Spectra 1- 3	41.4±5.0	11.1±2.2	3.7

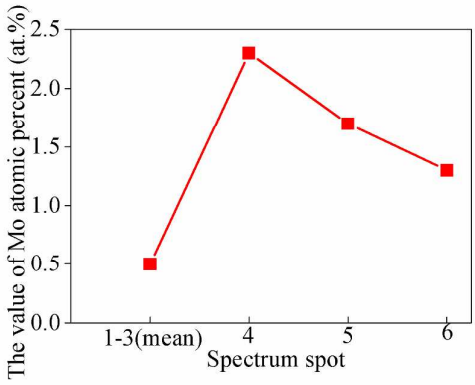

Fig. 9 The values of at. (%) of Mo of A0M5 mullite membrane support sintered at 1200 °C (from Fig. 8c).

Fig. 8 and Table 4 demonstrate the SEM-EDS analysis results of the fracture surface of the A0M0, A4M0, A0M5 and A4M5 membrane supports sintered at 1200 °C. For A0M0 sample, it is found that porous structure is formed by partial-sintering of mixture particles of fly ash and bauxite without much morphological change at 1200 °C. The EDS analysis, conducted on spots 1, 2 and 3 (Spectra 1, 2 and 3 in Fig. 8a) reveals that the mullite sintered particle fabricated in A0M0 at 1200°C show a slightly lower average molar ratio of Al to Si (~2.5) (Table

4) than the theoretical value (3.0) of stoichiometric mullite ($3Al_2O_3 \cdot 2SiO_2$). In a mullite precursor consisting of oxides, densification occurs before the mullite formation, which is known as the transient viscous sintering [38], so that the dissolution of Al_2O_3 is very difficult. There may be residual amorphous SiO_2 left in the samples. Therefore, it is difficult for mullite crystals to grow anisotropically and no mullite whiskers appear in this case [39].

Well-developed mullite whiskers are formed especially in the MoO_3-doped and AlF_3- MoO_3-codoped samples (Figs. 8c, 8d). It is expected that the excess SiO_2 is consumed by the Al_2O_3 precursors, mullite whiskers are totally formed and mullite phase becomes dominant in the sample sintered at 1200 °C. The pore structure and stiff skeleton needle-like structure mullite forms *in situ* [40], these inter-locked mullite whiskers are expected to exhibit excellent mechanical properties such as high strength (consistent with the above BFS results) and high modulus since they absorb much higher fracture energies than partially-sintered glassy phase particles (in spite of with fine elongated mullite crystals embedded), and consequently resulting in an enhancement in mechanical strength [21, 27]. This also would make support have a good pore structure as reported by Okada *et al.* [40].

In the sample (Fig. 8b) doped with 4 wt. % AlF_3 (A4M0), several elongated mullite crystals with different sizes are found in the matrix consisting primarily of the thinner ones. In some locations (on spots 1, 2, 3 and 4 in Fig. 8b), very high levels of Al are detected, giving a ratio of Al to Si of about 4.0, 4.0, 3.8 and 3.4, with an average value of 3.8 (Table 3), which is much higher than that of theoretical value (3.0) of mullite ($3Al_2O_3 \cdot 2SiO_2$). This result indicates a SiO_2 deficient composition with respect to stoichiometric mullite. This formation of Al_2O_3-rich mullite in A4M0, similar to A4M5 as discussed below, is ascribed to the evaporation of the SiO_2 component at high temperature based on the reaction equations (equations 3-6) given below.

For A0M5 (Fig. 8c), an average ratio of Al to Si of about 3.1 (2.9, 3.3 and 3.2 of the region marked as spectra 1, 2 and 3), which is quite close to the theoretical value of 3.0 indicating that the elongated whiskers are composed of stoichiometric mullite. Several growth mechanisms of ceramic whiskers have been reported in the previous studies [41, 42]. The growth mechanism can be identified based on the intervention of a metal catalyst, which exists in the system as an intentionally added catalyst. If the catalyst participates in the growth of the whiskers, it results in metal beads at the tips of the whiskers (vapor–liquid–solid growth mechanism) or nanosized metal impurity phases inside of the whiskers (two-stage growth mechanism). As shown in Fig. 8c (Spectra 4, 5 and 6), careful observation of the mullite whiskers using SEM shows there are metal beads at the tips of the whiskers in the A0M5 membrane support.

The average value (1.8%) of Mo atomic percent (at.%) at the tips of the whiskers is two time higher than that (0.5%) at the middle of the whiskers of spectrum 1, 2 and 3 as Fig. 9 shows. This observation indicates that the whiskers have grown with a metal catalyst (MoO_3), and therefore a vapor-liquid-solid growth mechanism plays an important role in the growth of mullite whiskers.

The mullite whiskers fabricated in the A4M5 (Fig. 8d) membrane support show a higher molar ratio of Al to Si (3.5, 3.5 and 4.1 of spectra 1, 2 and 3) than the theoretical value of 3.0. The measured composition is quite similar to that in a previous study [43], where mullite whiskers synthesized via the vapor-phase reaction induced by AlF_3 and an Al_2O_3-rich mullite (64.7 mol % Al_2O_3) was ultimately obtained. This formation of slightly Al_2O_3-rich mullite is ascribed to the evaporation of the SiO_2 component at high temperature based on the reaction equations below [43].

$$6AlF_3 + 3O_2 \rightarrow 6\,AlOF + 12F \quad (5)$$

$$Al_2O_3 + 2F \rightarrow 2\,AlOF + 0.5O_2 \quad (6)$$

$$2SiO_2 + 8F \rightarrow 2SiF_4 + 2O_2 \quad (7)$$

$$6AlOF + 2SiF_4 + 3.5O_2 \rightarrow 3\,Al_2O_3.2SiO_2 + 14F \quad (8)$$

AlF_3 is considered to be oxidized to AlOF. The released fluoride anion via reaction (Eq. 5) attacks Al_2O_3 and SiO_2 to form AlOF and SiF_4, respectively. The mullitization process can be significantly accelerated by AlF_3. The EDS analysis, conducted on spot 4 (Spectrum 4 in Fig. 8d) of fracture surface reveals that the mullite whiskers show a slightly SiO_2-rich composition as compared to 3:2 mullite, which may be ascribed to the excessive growth of mullite nuclei through liquid phase caused the entrapment of coal-fly-ash-derived SiO_2 within mullite crystals.

The stable crystal structure of mullite is orthorhombic with lattice constants a= 7.545 A˚, b= 7.689 A˚ and c= 2.884 A˚, and it consists of edge-shared AlO_6 octahedralchains aligned in the c-direction and cross-linked by cornershared $(Si,Al)O_4$ tetrahedra [44]. Due to its anisotropic unit cell structure, mullite has a strong tendency to grow anisotropically if the formation-growth of mullite grains takes place without any constraint [45]. Thus, the crystal growth maybe faster in crystallographic direction parallel to the c-axis than any other directions, resulting in a high degree of orientation,

The morphology of original mixture powder in the precursor is in flake-like shape. In the case of MoO_3 addition well developed mullite whiskers formed. In presence of MoO_3, the glass phase rich in low melting components will have a lower eutectic temperature and a reduced viscosity. So at lower temperature, a liquid phase is developed which can reduce the mullitization temperature considerably by minimizing the viscosity of the SiO_2-rich liquid phase of the samples. The excess SiO_2 in fly ash is thus consumed rapidly by Al_2O_3 and large crystals of secondary mullite are formed at 1200 °C. The reduced temperature of mullite phase formation due to the addition of MoO_3 in the present work can also be detected by XRD. Due to the lowering of mullitization temperature, mullite grains grow without significant occurrence of densification. Therefore, the mullite grains have

a strong tendency of anisotropic growth as the grain growth is under an unconstrained environment. In such case, the whiskers grow preferentially along the parallel direction to the c-axis, resulting in an orthorhombic structure [46]. As a result, the mullite crystal grows into needlelike morphology. The growth of whisker-structured mullite crystals can be explained on the enhanced formation and lower melting point of a secondary glass phase, allowing an enhanced solution-precipitation process in the glass.

3.3.4 TEM

As a result of this study, the EDS results indicate that there is an obvious variation of Si/Al ratio on different whiskers and even within one single whisker. The mullite whiskers, which have an average molar ratio of Al/Si from 3.1 to 3.8 in this work (see Table 4), is in the theory mullite range, possibly be due to a mixture of whiskers of different compositions. In addition to the errors caused by the raw material, it should be noticed that errors can be generated in the semi-quantitative analysis of elements using the methodology to determine the chemical composition by EDS, since the EDS analysis sometimes takes in the background materials which could derive from the materials other than the whiskers.

The phase structure of whiskers is identified by SAED based on TEM. One SAED pattern for mullite is shown in Fig.10. As can be seen from Fig. 10, the crystal structure of the whiskers is shown by observation of TEM and microbeam diffraction (Fig. 10), to be orthorhombic, the orthorhombic type mullite whiskers are also reported by [20,47].

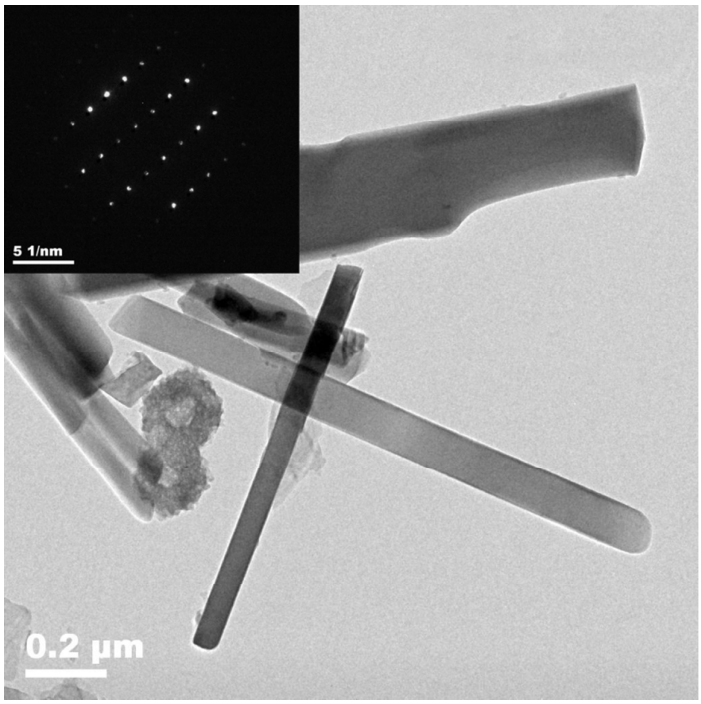

Fig 10. TEM micrograph and microbeam diffraction of mullite whiskers obtained by sintering membrane support of coal fly ash and bauxite, with an addition of 4 wt. % AlF_3 and 5 wt. % MoO_3, at 1200 °C for 2 h.

3.3.5 XRD

Fig. 11 shows the XRD patterns of the A0M0, A4M0, A0M5 and A4M5 membrane supports. For A0M0, the peak intensity of corundum, decomposed from the diaspore in bauxite decreases gradually due to its dissolution into a transient liquid phase for further secondary mullitization reaction from 1100 to 1300 °C [48]. At 1300 °C, besides mullite (PDF#15-0776) and corundum (PDF#10-0173), the cristobalite (PDF#27-0605) in the A0M0 membrane support is also detected. The dependence of mullite phase content on sintering temperature based on RIR analysis (Fig. 12) shows the mullite content in A0M0 (32%) at 1100 °C is lower than that in AlF_3- and MoO_3-doped samples (A4M0, 42%; A0M5, 37%; and A4M5, 48%). It should be noted, the content of mullite in the precursor mixture of coal fly ash and bauxite is 18%, so after calculation, the contents of mullite which is produced because of the reaction between cristobalite and diaspore-derived corundum of A0M0, A4M0, A0M5 and A4M5 are 14%, 24%, 19% and 32%, respectively.

The mullite content of A0M0 increases rapidly from 25% to 76% from 1100 to 1300 °C, indicating that the mullitization mainly occurs over this temperature range. At higher temperature (1400 °C), the mullite content (79%) changes very little. The mullite content of A4M0 shows a similar trend with A0M0, firstly rapidly increases from

42% to 68% from 1100 to 1300 °C, then almost keep constant (70%) at 1400 °C, indicating that the mullitization is almost completed at 1300 °C. Nevertheless, in this work the diffraction peaks of corundum are still observed even after sintering at 1400 °C. It is probably because the alumina in coarse bauxite (d_{50}= 1.22 μm) is of low reaction activity, resulting in a longer dynamic reaction diffusion path between bauxite-derived alumina and coal-fly ash-derived silica [33].

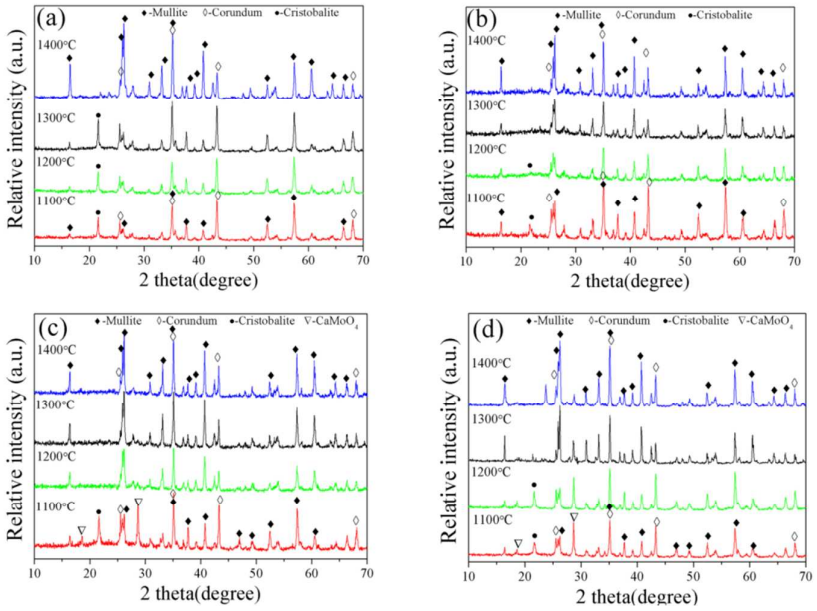

Fig. 11 XRD patterns of the A0M0 (a), A4M0 (b), A0M5 (c) and A4M5 (d) membrane supports sintered at various temperatures for 2 h (●-Cristobalite, ∇-$CaMoO_4$, ◊-Corundum, ◆-Mullite).

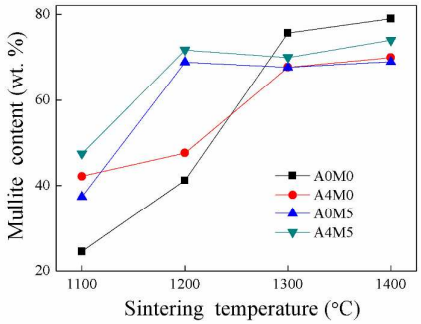

Fig. 12 Effect of sintering temperature on mullite content in the A0M0, A4M0, A0M5 and A4M5 membrane supports.

For the samples with 5 wt. % MoO_3 (A0M5), a dramatically increase in mullite content from 37% to 69% due to the rapid formation of secondary mullite from 1100 °C-1200 °C. The content of mullite does not significantly increase at the temperatures between 1200 °C and 1400 °C (70%), the cristobalite (PDF#27-0605) is not detected in the A0M5 membrane support, revealing that the presence of MoO_3 is effective in promoting secondary mullitization at lower temperatures (1200 °C). It can be attributed to the fact that MoO_3 promoted the growth of anisotropic mullite crystals by reducing the high-temperature viscosity of the MoO_3-containing liquid phase and consequently increasing the crystal growth rate during the sintering process.

For the A4M5 samples, the variation in phase content with sintering temperature is similar to that of A0M5, but the mullite content is slightly higher (72% at 1200 °C for A4M5 compared with 69% for A0M5). At higher sintering temperature (1300 and 1400 °C), the mullite content remains in the range of 71%-74% above 1200 °C, which indicates that with 4 wt. % of AlF_3 and 5 wt. % of MoO_3 addition, secondary mullitization is almost complete at ~1200 °C, is lowed 100 °C as compared with the samples without any additives.

3.4. Separation of oil-in-water emulsion by mullite membrane support

Fig. 13 Images of oil-in-water emulsion: before (left) and after (right) separation test.

Fig. 13 shows the appearance of oil-in-water emulsion samples before and after separation test. The appearance of oil-in-water emulsion has a slightly turbid, white and milky appearance before separation test. Once the mixture is filtrated through the mullite membrane support, the solution transforms from turbid to pellucid suggesting that the color change is due to high efficiency oil-in-water separation of mullite membrane support. TOC (total organic carbon) removal efficiency is higher than 90% at 0.2 MPa. As a follow-up to this work, a detailed and optimized investigation on separation of oily water using such membrane materials is being under way in order to achieve its environmental separation functions.

4. Conclusions

The mullite membrane supports with inter-locked whisker structure were prepared via recycling of an industrial waste, coal fly ash and bauxite in the temperature range of 1100-1400 °C, with addition of AlF_3 and MoO_3 as mineralizer and crystallization catalyst, respectively. It showed that introduction of MoO_3 effectively promoted the growth of elongated mullite whisker in the membrane support by reducing the high temperature viscosity of the liquid melt. Addition of 5 wt. % MoO_3 lowered secondary mullitization temperature, resulting in more mullite formation at temperature as low as 1200 °C, while porosity of 45.4±0.9% was obtained. After sintering at 1200 °C, open porosity was 47.3±0.6% for the sample containing 4 wt. % AlF_3. It was proposed that a vapor phase reaction between SiF_4 and AlF_3 resulted in synthesis of the elongated mullite whiskers. The co-introduction of MoO_3 and AlF_3 promoted formation of a porous whisker-interlocked structure, which effectively improved open porosity and gas flux without significant mechanical strength degradation. This study may provide an alternative method of recycling the coal fly ash waste not only to reduce its environmental impacts but to produce high-valued mullite-based porous ceramic membranes for potential oily water separation applications.

5. Acknowledgements

This work was financially supported by the Industry Leading Key Project of Fujian Province, China (No. 2014H0050), the National Natural Science Foundation of China (No. 21301171), the Natural Science Foundation of Fujian Province, China (No. 2014J01215) and Ningbo Natural Science Foundation, China (No. 2014A610004).

6. Notes and references

a. CAS Key Laboratory of Urban Pollutant Conversion, Institute of Urban Environment, Chinese Academy of Sciences, P. R. China
b. Ningbo Urban Environment Observation and Research Station-NUEORS, Chinese Academy of Sciences, P R China
c. School of Chemistry and Chemical Engineering, South China University of Technology, Guangzhou, P R China
d. Department of Environmental Engineering, Chung Yuan Christian University, Chung-Li, 320, Taiwan

[1] R. Blissett and N. Rowson, *Fuel*, 2012, 97, 1-23.
[2] J. Yu, X. Li, D. Fleming, Z. Meng and D. Wang, *Energy Proced.*, 2012, 17, 3-9.
[3] N.K. Koukouzas, R. Zeng, V. Perdikatsis, W. Xu and E.K. Kakaras, *Fuel*, 2006, 2301-2309.
[4] R.S. Iyer and J.A. Scott, *Conserv. Recycl.,* 2001, 31, 217-228.
[5] I. Jedidi, S. Khemakhem, A. Larbot and R. Ben Amar, *Ceram. Int.*, 2009, 35, 2747-2753.
[6] I. Jedidi, S. Saïdi, S. Khemakhem, A. Larbot, N. Elloumi-Ammar, A. Fourati, A. Charfi, A.B. Salah and R.B. Amar, *J. Hazard. Mater.*, 2009, 172, 152-158.
[7] Y. Dong, X. Liu, Q. Ma and G. Meng, *J. Membr. Sci.*, 2006, 285, 173-181.
[8] V.K. Jha, M. Matsuda and M. Miyake, *J. Hazard. Mater.*, 2008, 160,148-153.

[9] M. Ahmaruzzaman and V. Gupta, *Ind. Eng. Chem. Res.*, 2012, 5, 15299-15314.
[10] Y. Yoshino, T. Suzuki, B.N. Nair, H. Taguchi and N. Itoh, *J. Membr. Sci.*, 2005, 267, 8-17.
[11] T. Van Gestel, D. Sebold, H. Kruidhof and H.J. Bouwmeester, *J. Membr. Sci.*, 2008, 318, 413-421.
[12] S. Ananthakumar, M. Jayasankar and K. Warrier, *Acta. mater.*, 2006, 54, 2965-2973.
[13] H.J. Choi, J.G. Lee, *J. Am. Ceram. Soc.,* 2002, 85,481-483.
[14] H. Schneider, K. Okada, J.A. Pask, John Wiley and Sons, New York, 1994,158-159.
[15] A. Guo, J. Liu, R. Xu, H. Xu and C. Wang, *Fuel*, 2010, 89, 3630-3636.
[16] J.S. Jung, H.C. Park, R. Stevens, *J. Mater. Sci. Lett.* 20 (2001) 1089–1091
[17] J.-H. Li, H.-W. Ma and W.-H. Huang, *J. Hazard. Mater.*, 2009, 166, 1535-1539.
[18] S. Li, H. Du, A. Guo, H. Xu, D. Yang, , *Ceram. In*t., 2012,38,1027-1032.
[19] X. Huang, J.Y. Hwang, B.C. Mutsuddy, *Ceram. Int., 1*995, 44,65–71.
[20] Y. Park, T. Yang, S. Yoon, R. Stevens, H. Park, *Mater. Sci. Eng., A,* 2007,454,518-522.
[21] Y. Dong, S. Hampshire, J.-e. Zhou, Z. Ji, J. Wang and G. Meng, *J. Eur. Ceram. Soc.*, 2011, 31, 687-695.
[22] A.R. Studart, U.T. Gonzenbach, E. Tervoort and L.J. Gauckler, *J. Am. Ceram. Soc.*, 2006, 89, 1771-1789.
[23] J. Mueller, Y. Cen and R.H. Davis, *J. Membr. Sci.*, 1997, 129, 221-235.
[24] T. Ohji and M. Fukushima, *Int. Mater. Rev.*, 2012, 57, 115-131.
[25] C. Nischik, M.M. Seibold, N.A. Travitzky and N. Claussen, *J. Am. Ceram. Soc.*, 1991,74, 2464-2468.
[26] P. Peng and C. Sorrell, *Mater. Lett.*, 2004, 58, 1288-1291.
[27] Y. Park, T. Yang, S. Yoon, R. Stevens and H. Park, *Mater. Sci. Eng., A*, 2007, 454, 518-522.
[28] F.H. Chung, *J. Appl. Crystallogr.*, 1974, 7, 526-531.
[29] A. Hernández, J. Calvo, P. Prádanos and F. Tejerina, *J. Membr. Sci.*, 1996, 112 , 1-12.
[30] S. Timoshenko, S. Woinowsky-Krieger and S. Woinowsky, McGraw-hill, New York, second ed., 1959.
[31] W.A.J. Higgs, P. Lucksanasombool, R.J.E.D. Higgs and M.V. Swain, *Biomaterials*, 2001, 22, 1583-1590.
[32] X. Zhong, G. Li, H.S. Chung and K.P. Li, *Ceram. Int.*, 1981,7, 65-68.
[33] Y. Dong, J.-e. Zhou, B. Lin, Y. Wang, S. Wang, L. Miao, Y. Lang, X. Liu and G. Meng, *J. Hazard. Mater.*, 2009, 172 , 180-186.
[34] G. Chen, H. Qi, W. Xing and N. Xu, *J. Membr. Sci.*, 2008, 318, 38-44.
[35] Y.H. Wang, Y. Zhang, X. Liu and G.Y. Meng, *Powder technol.*, 2006, 168 ,125-133.
[36] W. Weibull, *J. Appl. Mech.*, 1951.
[37] X. Fan, E.D. Case, I. Gheorghita and M.J. Baumann, *J. Mech. Behav. Biomed. Mater.*, 2013, 20, 283-295.
[38] M.D. Sacks, N. Bozkurt and G.W. Scheiffele, *J. Am. Ceram. Soc.*, 1991, 74, 2428-2437.
[39] L. Kong, H. Huang, T. Zhang, Y. Gan, J. Ma, F. Boey and R. Zhang, M*ater. Sci. Eng., A*, 2003, 359, 75-81.
[40] K. Okada and N. Ōtuska, *J. Am. Ceram. Soc.,* 1991, 74, 2414-2418.
[41] H.-J. Choi and J.-G. Lee, *Ceram. Int.,* 2000, 26, 7-12.
[42] S.R. Nutt, *J. Am. Ceram. Soc.,* 1988,71,149-156.
[43] K. Okada and N. Ōtsuka, *J. Mater. Sci. Lett.,* 1989, 8, 1052-1054.
[44]J.Y. Jaaski, H.U. Nissen, *Phys. Chem. Miner.*, 1983, 10, 47-54.
[45] S.H. Hong, W. Cermignani, G.L. Messing, *J. Eur. Ceram. Soc.,* 1996, 16, 133.
[46] L.B. Kong, H. Huang, T.S. Zhang, J. Ma, F. Boey, R.F. Zhang, Z.H. Wang, *J. Eur. Ceram. Soc.*, 2003, 23, 2257-2264.
[47] Y.-F. Chen, M.-C. Wang, M.-H. Hon, *J. Eur. Ceram. Soc.,* 2004, 24, 2389-2397.
[48] M.A. Sainz, F.J. Serrano, J.M. Amigo, J. Bastida and A. Caballero, *J. Eur. Ceram. Soc.,* 2000, 20, 403-412.

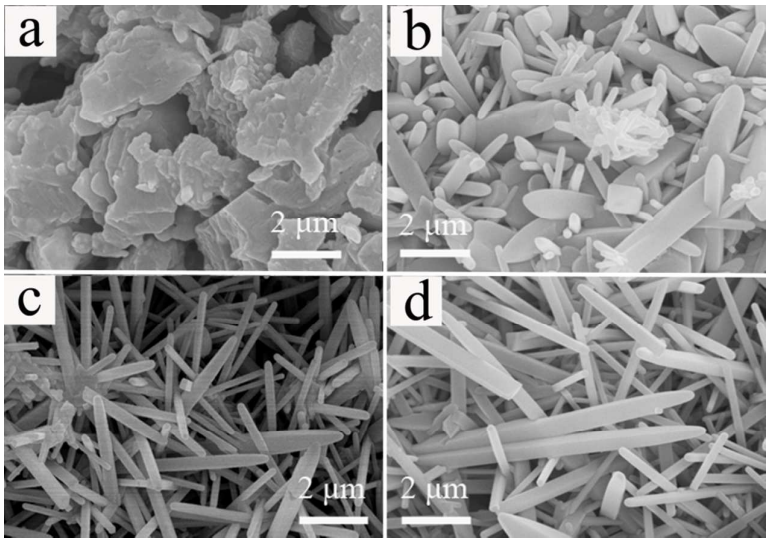

SEM images of mullite membrane support (a) without addition, (b) with addition of AlF_3, (c) with addition of MoO_3 and (d) with addition of AlF_3 and MoO_3.